Shielding properties of laser-induced breakdown in water for pulse durations from 5 ns to 125 fs

Daniel X. Hammer, E. Duco Jansen, Martin Frenz, Gary D. Noojin, Robert J. Thomas, Joachim Noack, Alfred Vogel, Benjamin A. Rockwell, and Ashley J. Welch

The shielding effectiveness of laser-induced breakdown from focused, visible laser pulses from 5 ns to 125 fs is determined from measurements of transmission of energy through the focal volume. The shielding efficiency decreases as a function of pulse duration from 5 ns to 300 fs and increases from 300 fs to 125 fs. The results are compared with past studies at similar pulse durations. The results of the measurements support laser-induced breakdown models and may lead to an optimization of laser-induced breakdown in ophthalmic surgery by reduction of collateral effects. © 1997 Optical Society of America

Key words: Laser-induced breakdown, optical breakdown, plasma, shielding, intraocular photodisruption.

1. Introduction

Laser-induced breakdown (LIB) has been used since 1980 in ophthalmic surgery to rupture tissue in the posterior capsule subsequent to cataract surgery[1–4] and in the iris to relieve intraocular pressure as a treatment for glaucoma.[5–7] In addition, new medical treatments are under investigation that use LIB in various ophthalmic applications[8] and other areas of the body.[9–12] There are also nonmedical applications of LIB such as hazardous waste identification by spectroscopy (time-resolved laser-induced breakdown spectroscopy[13]) and optical limiting.[14]

LIB is initiated by either avalanche ionization (for long pulse durations) or multiphoton ionization (for short pulse durations) of molecules such that plasma forms. One of the characteristics of LIB that allows it to be used beneficially is its ability to shield a significant portion of the input energy, thereby limiting the amount of energy that can cause unwanted damage beyond the focus (especially at the retina). The term "shielding" used throughout this paper is equivalent to the total pulse energy minus the transmitted energy (or transmittance). The amount of light shielded by the plasma depends on input energy, laser-pulse duration, wavelength, spot size at focus, and cone angle. The energy shielded is lost by one of three mechanisms: absorption, reflection, or scatter. The energy absorbed by the plasma generates very high temperatures (>5000 K) within the plasma[15] and results in shock waves and cavitation bubbles.[16] Many studies have sought to quantify the amount of energy that is coupled by the plasma into the shock waves and cavitation bubbles.[17–19] The energy may also be scattered backward (such as in stimulated Brillouin scattering[20]) or reflected by the optically dense plasma. In addition, other nonlinear effects may take place as the pulse duration decreases, such as self-focusing[21] and continuum generation.[22] For this paper we are concerned only with the amount of energy transmitted through the plasma as a function of the input energy and pulse duration.

For potential laser surgical uses that employ femtosecond LIB, it is still not clear exactly which mechanism causes tissue rupture. For example, very high temperatures within the plasma may cause a thermal response that essentially vaporizes the tissue, or high peak pressures caused by the shock waves may cause damage in the focal region where the pressures are highest. Alternatively, the dam-

D. X. Hammer and A. J. Welch are with the Biomedical Engineering Program, University of Texas, Austin, Texas 78712. E. D. Jansen is with the Biomedical Engineering Department, University of Vanderbilt, Nashville, Tennessee 37235. M. Frenz is with the Institute of Applied Physics, University of Bern, Switzerland. G. D. Noojin and R. J. Thomas are with TASC, 750 East Mulberry Street, Suite 302, San Antonio, Texas 78212. J. Noack and A. Vogel are with the Lübeck Medical Laser Center, Lübeck, Germany. B. A. Rockwell is with the Optical Radiation Division, Armstrong Laboratory, Brooks Air Force Base, Texas 78235.

Received 11 December 1996; revised manuscript received 2 January 1997.

0003-6935/97/225630-11$10.00/0

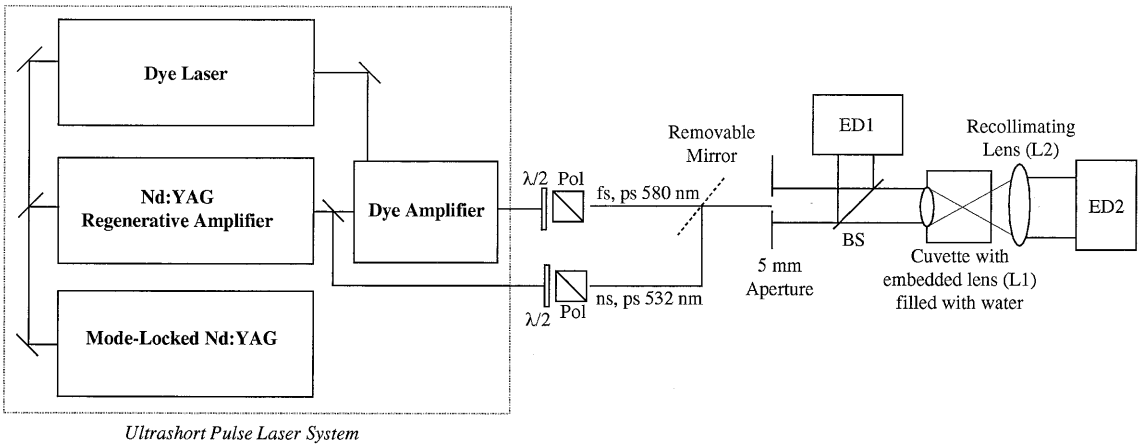

Fig. 1. Optical setup used to measure shielding of laser-induced breakdown. Pol, polarization cube; ED, energy detector; BS, beam splitter; λ/2, half-wave plate. See Ref. 29 for a full description of the ultrashort-laser-pulse system.

age may be caused by movement of material that occurs on longer time scales with cavitation bubble expansion and oscillation (collapse and reexpansion). Cavitation has been found to be the main cause of tissue rupture for nanosecond and picosecond pulses.[18,19] In addition, the role that several nonlinear mechanisms (like those listed above) play in tissue damage needs to be fully characterized. Further research is necessary to explain the exact damage mechanisms caused by LIB.

Whatever is the mechanism for damage, one goal of the current research into LIB is to localize tissue damage at the beam focus and thereby reduce collateral damage (caused either by shock waves or cavitation bubbles) away from the breakdown site. To that end, many researchers have proposed using shorter laser-pulse durations by which collateral damage is greatly reduced.[16,18,23–27] Preliminary evidence suggested that the shielding effectiveness also increases as the pulse duration decreases[24]; however, results to the contrary have also been reported.[28] If the shielding effectiveness of LIB decreases for shorter pulse durations, a deleterious increase in energy throughput beyond the focal plane to critical structures (such as the retina) may accompany the reduction in collateral mechanical damage. The ability of shielding to protect posterior tissue has been reported in the literature for nanosecond and picosecond pulse durations.[24,25,28–36] We present a measurement of the shielding properties of LIB for pulse durations that range from 5 ns to 125 fs. The results lend insight to physical interpretations of ultrashort pulse LIB in water and similar liquids.

2. Materials and Methods

The setup used for measurement of laser-light transmission through the focal volume is shown in Fig. 1. The ultrashort-pulse laser system has been described previously.[29] We used 5-ns and 60-ps pulses at 532 nm, and 3-ps, 300-fs, and 125-fs pulses at 580 nm. The pulses were monitored temporally either by autocorrelation (Inrad Autocorrelator) or with a fast photodiode (risetime <1 ns) and oscilloscope, and the energy output was controlled by a half-wave plate and a polarization cube. A 5-mm-diameter aperture in front of the beam splitter limited the effects of spherical aberrations by the focusing lens and provided a constant beam diameter and cone angle for two different laser-output-beam diameters (11 mm at 532 nm and 6 mm at 580 nm at the $1/e^2$ point). There was some danger in aperturing the beam in that the Gaussian profile may become a truncated Gaussian or top-hat profile for small apertures. Although aperturing the beam did not significantly affect our setup with respect to shielding, it did account for a small difference in the measured spot size. The spot size (diameter) was measured in water at the beam waist with the knife-edge technique[37] and was found to be 10.8 ± 1.0 μm for 580 nm and 7.2 ± 1.0 μm for 532 nm. With the 5-mm-aperture and 17-mm-focal-length lens, the input focusing (full) angle was 16.7°. After the aperture, the beam was split and the input energy (E_{in}) was measured on the front energy detector (Molectron JD2000 Joulemeter Ratiometer and various pyroelectric heads) and corrected for the beam-splitter ratio. The remainder was sent to a cuvette that held triply deionized, high-purity water. The cuvette was built to hold a lens (L1, 17-mm focal length in water, 1.784 linear refractive index at 580 nm) custom designed to focus light from air to water with minimal aberrations. The reduction in aberrations was achieved in large part by the high-refractive-index glass of the lens. The transmitted light was then collected with a lens (L2, 70-mm focal length in air, 1.5 linear refractive index for 580 nm) and the output energy (E_{out}) measured with the energy detector behind the cuvette (ED2). The distance from the plasma to the back lens was approximately 50 mm and the working diameter of the lens was 43 mm. Therefore the output collimating (full) angle was 46.5°. This cone angle was sufficient to collect all light transmitted through the focal region, including the light scattered in the forward direction. Shielding was measured by compar-

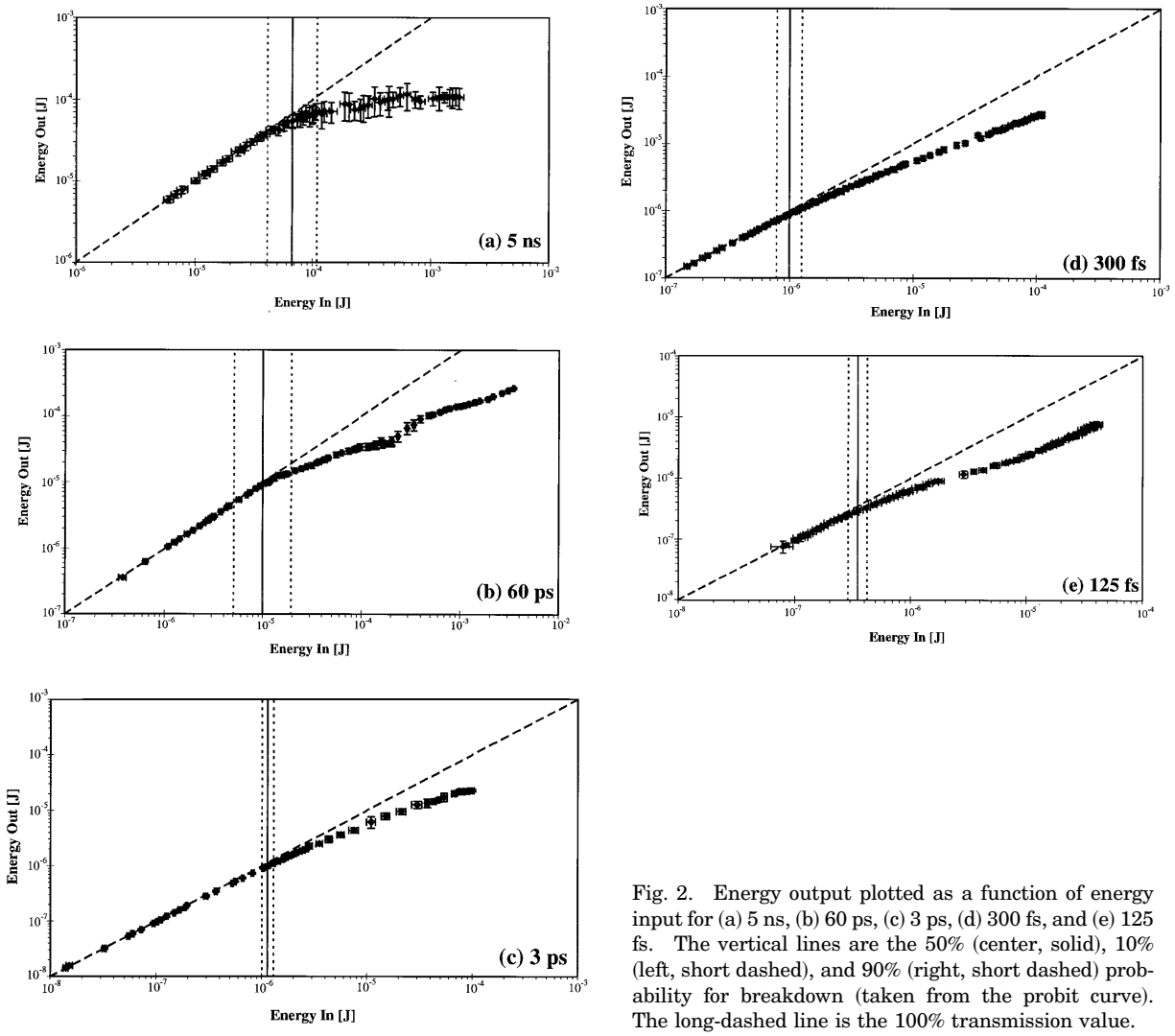

Fig. 2. Energy output plotted as a function of energy input for (a) 5 ns, (b) 60 ps, (c) 3 ps, (d) 300 fs, and (e) 125 fs. The vertical lines are the 50% (center, solid), 10% (left, short dashed), and 90% (right, short dashed) probability for breakdown (taken from the probit curve). The long-dashed line is the 100% transmission value.

ing the collimated light prior to breakdown with the collimated light after breakdown corrected for Fresnel reflections and water absorption.

The energy threshold for LIB (E_{thres}) was measured by statistical analysis of 200 single-shot pulses. For each shot, breakdown was determined by observing cavitation events in the focal region when illuminated by the probe pulse perpendicular to the pump pulse at a fixed time (1 μs) after breakdown. The probe pulse was monitored with a CCD digital camera (Cohu, Inc.). When breakdown occurred, a cavitation bubble was clearly visible on the monitor connected to the camera. The cavitation bubble has been used previously as an end point for breakdown.[38] Probit analysis was used to generate a probability curve for breakdown. Probit analysis is a statistical analysis used to quantify dose percentages (estimated doses, or ED) where results are binary (i.e., yes, there is breakdown, or no, there is no breakdown). The threshold is defined in this report as the estimated energy dose giving a 50% probability (or ED_{50}) of breakdown.

3. Results

Figure 2 is a plot of the output energy (E_{out}) as a function of input energy (E_{in}) for each pulse duration. Each point in Fig. 2 represents an average of 25 measurements at a particular input energy. The standard deviation for the 25 measurements of output energy and input energy is shown as horizontal and vertical error bars, respectively. The vertical lines are the 50% probability threshold (solid line) and the 10% and 90% probability thresholds (short dashed lines, 10% to the left and 90% to the right). The long dashed line shows the point where input energy and output energy are equal (i.e., 100% transmission).

The shielding data as measured by energy transmission for each pulse duration is shown in Fig. 3. The percent transmission ($E_{\text{out}}/E_{\text{in}}$), corrected for Fresnel reflections that are due to index mismatches in the setup, is plotted as a function of the ratio of the input energy to the energy threshold for breakdown ($\beta = E_{\text{in}}/E_{\text{thres}}$). The normalized pulse energy β is used to compare data for different pulse durations. The error in transmission (square root of the sum of the squares of the standard deviation of the 25 mea-

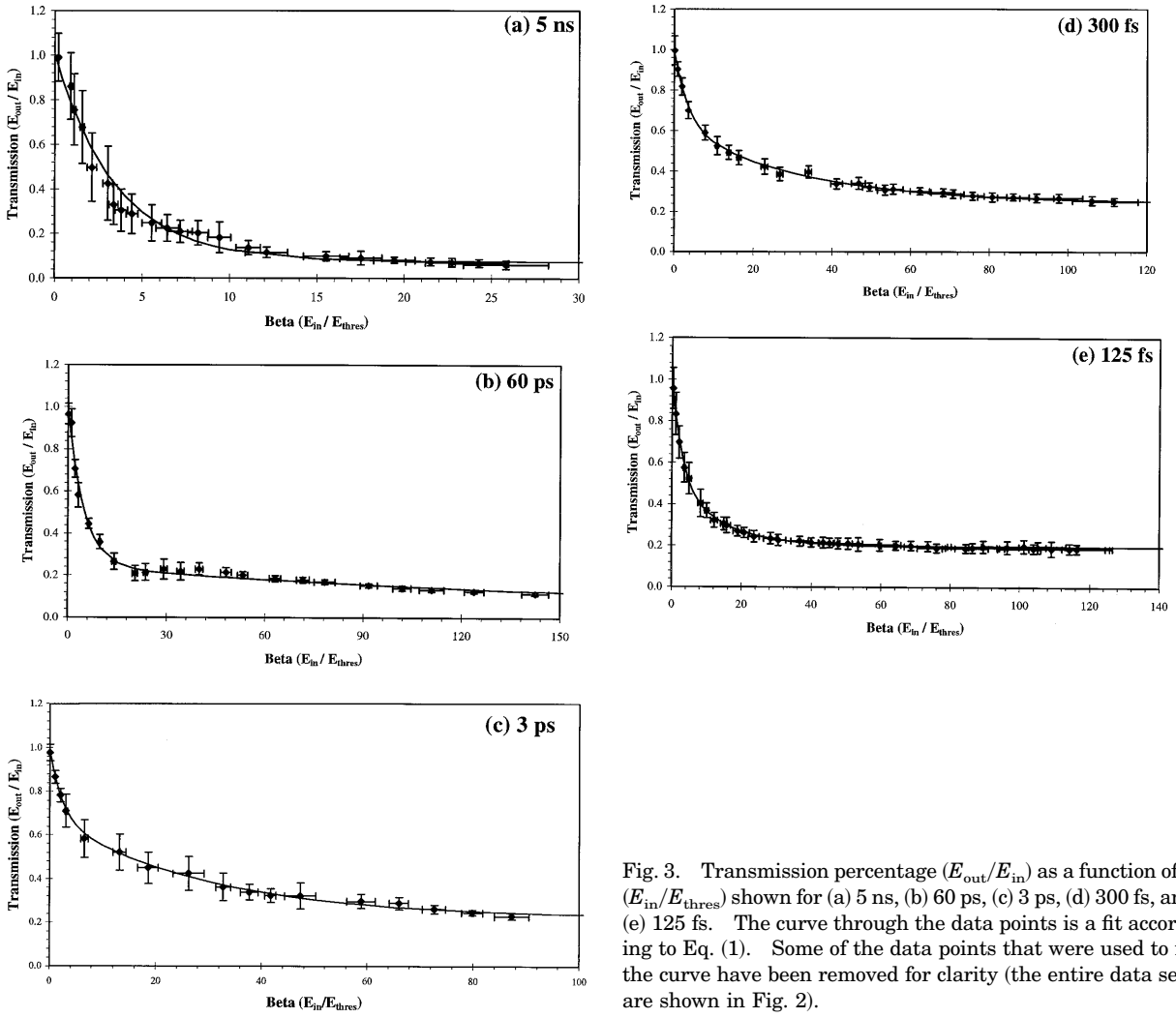

Fig. 3. Transmission percentage (E_{out}/E_{in}) as a function of β (E_{in}/E_{thres}) shown for (a) 5 ns, (b) 60 ps, (c) 3 ps, (d) 300 fs, and (e) 125 fs. The curve through the data points is a fit according to Eq. (1). Some of the data points that were used to fit the curve have been removed for clarity (the entire data sets are shown in Fig. 2).

surements of input and output energy for each data point) and the error in β (standard deviation of the input energy) are shown as horizontal and vertical error bars, respectively. The line through each data set represents an empirical fit (least-squares method) of the data to a double exponential curve described by

$$\text{Transmission} = a + b[\exp(-c\beta)] + d[\exp(-e\beta)]. \quad (1)$$

The coefficient a in the above equation represents the transmission percent to which the curves level off, i.e., the minimum transmission (maximum shielding), coefficients c and e represent the slope of the curve, and coefficients b and d describe the relative importance of the two parts of the exponential decay. The sum of coefficients a, b, and d should thus be 1 for $\beta = 0$. All coefficients are dimensionless and are empirically determined parameters of the fit. R^2 was greater than 0.99 for each fit.

The physical significance of the double exponential is not known at this time, but we speculate that it is derived from the interplay of two circumstances. One exponential with a steep slope describes the transition from plasma near threshold (very small plasma length and nonabsorbing) to plasma for large β (long plasma length and highly absorbing). The second exponential with a final flat slope describes the fact that the plasma is not 100% absorbing for large β.

Table 1 lists the threshold and transmission values for each pulse duration. Both the energy threshold at three different points on the probability curve and the irradiance threshold calculated from the 50% energy threshold are shown. The transmission value at $\beta = 100$ (from the above fit) is listed to show the shielding trend as a function of pulse duration.

The error bars in Figs. 2 and 3 indicate pulse-to-pulse energy fluctuations of the laser during measurement and were particularly large for 5 ns but generally remained below 10%. The shape of the transmission curves remained the same for all pulse durations, even for the noisy 5-ns data. There was a slight hump in the 60-ps data near $\beta = 30$ [Fig. 3(b)]. However, the error bars also increased significantly at that point. As expected, Fig. 2 indicates that for all pulse durations, the data separates from 100% transmission near threshold. The shape of the curve greater than threshold is generally linear, al-

Table 1. Some Parameters of Laser-Induced Breakdown and Shielding Found for Pulse Durations from 5 ns to 125 fs

Pulse Duration (Wavelength)	Threshold[a] Energy [μJ] 10%	50%	90%	Irradiance [W/cm^2] (with 50% threshold)	Transmission[b]
5 ns (532 nm)	41.4	67.2	109	3.30×10^{10}	0.074
60 ps (532 nm)	5.1	10.0	19.5	4.07×10^{11}	0.149
3 ps (580 nm)	1.0	1.1	1.3	4.15×10^{11}	0.238
300 fs (580 nm)	0.8	1.0	1.3	3.60×10^{12}	0.259
125 fs (580 nm)	0.29	0.35	0.42	3.06×10^{12}	0.194

[a]The energy threshold was found from probit analysis and the irradiance threshold was calculated from measurement of energy threshold, spot size diameter (measured at energies well below the threshold), and pulse duration.
[b]Transmission value is from the fit described by Eq. (1) at $\beta = 100$.

though there are some inflection points in the 125-fs and 60-ps data.

Figure 4 replots the fits for all pulse durations from Fig. 3 to allow for a comparison between pulse durations and to extrapolate to energies higher than the range measured. The inset of Fig. 4 shows the transmission curves for $\beta \leq 5$. For both large and small values of β, the transmission increases (shielding decreases) for pulse durations from 5 ns to 300 fs and decreases (shielding increases) for pulse durations from 300 fs to 125 fs. Because of our definition of breakdown (50% probability), the transmission is less than 100% for $\beta < 1$. 100% transmission occurs only when the probability for breakdown is 0%.

Figure 4 clearly shows that the shielding is most effective for 5-ns pulses relative to the other pulse durations measured in this study. At this pulse duration, the transmission curve has both the steepest slope and the lowest final value. The shielding efficiency as measured by the minimum transmission decreases from 5 ns to 300 fs. As the pulse duration is further decreased from 300 fs to 125 fs, the shielding efficiency increases. Thus there is a turning point at 300 fs in our experiment where the shielding efficiency reverses relative to pulse duration.

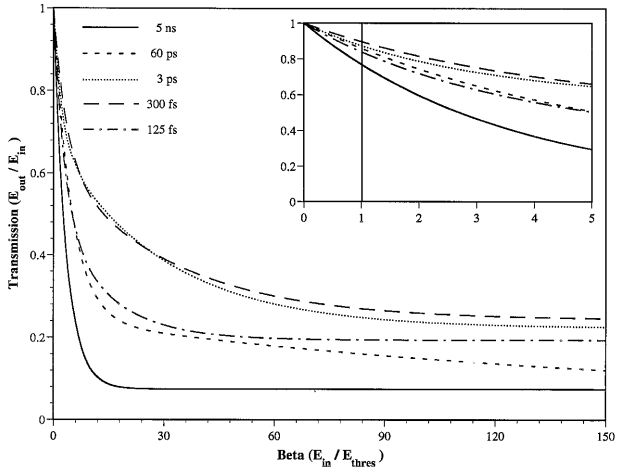

Fig. 4. Replot of the fits from Fig. 3. The inset shows the transmission for $\beta < 5$.

4. Discussion

An explanation of the shielding trends that we have observed as a function of pulse duration needs to include three points. First, differences between the observations made in this paper and those made in past papers must be explained. Since early investigations by Docchio and co-workers[24,31] indicated that shielding is more efficient for picosecond pulses than nanosecond pulses, this may be the most important consideration in this paper. Second, the decrease in shielding efficiency from nanosecond to picosecond pulse durations must be explained physically. Third, the reversal in the shielding efficiency in the femtosecond regime must be explained physically. The following subsections address each of these considerations in order.

A. Comparison with Past Studies

When LIB was first used for intraocular surgery, little was known about the dynamics of the breakdown process in liquids. In the past fifteen years, many studies have been reported in the literature regarding LIB in ocular and aqueous media, led most notably by Franco Docchio and Alfred Vogel. There have been several papers on shielding of plasmas produced by means of *Q*-switched (nanosecond) and modelocked (picosecond) Nd:YAG pulses.[24,25,28–36] With the exception of two preliminary conference proceedings articles from our laboratory,[29,38] to our knowledge no paper has reported on shielding by femtosecond pulses. Although the focusing characteristics and other experimental parameters differ in each of the past papers, an attempt will be made to compare the trends found in the past studies with those found in this study.

Table 2 lists the conditions and results of several past studies of shielding.[24,25,28,29,31,32,36] The data listed in Table 2 are taken directly from each paper with the exception of the spot sizes for the setup used by Boppart *et al.*,[29] which were measured after the paper was published and the spot sizes for the setup used by Docchio and co-workers,[24,31] which were converted from $1/e$ values to $1/e^2$ values (for comparison with other studies). As can be seen, there is considerable information missing from several of the pa-

Table 2. Comparison of the Experimental Parameters and Transmission Percent (E_{out}/E_{in}) for Various Studies near Breakdown Threshold

Study	Focal Characteristics: Spot Diameter (μm)	Focal Characteristics: Full Focusing Angle	Pulse Duration (Wavelength)	Media	β	% Transmission (E_{out}/E_{in})
Boppart[29]	~25	NA[a]	10 ns (1064 nm)	High-purity water	1	46 ± 4
		NA[a]	5 ps (580 nm)		1	27 ± 5
			100 fs (580 nm)		1	64 ± 11
Chekalin[25]	140	NA[a]	10 ns (1064 mm)	Distilled water	6	71
			30 ps (1064 nm)		6	7
Docchio[31]	NA[a,b]	3.5°	7 ns (1064 nm)	Saline	2	45
Docchio[24]	NA[a,b]	3.5°	7 ns (1064 nm)	Saline	1	57
					2	33
			220 ps (1064 nm)		1	50
					2	20
			30 ps (1064 nm)		1	41
					2	15
Mainster[32]	50	11°	22 ns (1064 nm)	Water	3.3	15
				Saline	1	32
			30 ps (1064 nm)[d]	Water	16.2	17
				Saline	1	44
Nahen[36]	7.6	22°	6 ns (1064 nm)	Distilled water	2	28
	11.5	8°			2	21
	4.7	22°	30 ps (1064 nm)		2	63
	9.6	8.5°			2	68
	19.5	4°			2	76
Steinert[28]	NA[a,c]	NA[a]	15 ns (1064 nm)	Saline	6	15
			15 ns (532 nm)		6	17
			25 ps (1064 nm)[e]		28	24
Present study	7.2	16.7°	5 ns (532 nm)	High-purity water	1	81 ± 16
					2	54 ± 16
			60 ps (532 nm)		1	92 ± 7
					2	73 ± 4
	10.8		3 ps (580 nm)		1	87 ± 3
					2	79 ± 3
			300 fs (580 nm)		1	89 ± 4
					2	82 ± 4
			125 fs (580 nm)		1	83 ± 10
					2	70 ± 8

[a]NA, not available.
[b]The spot diameter was probably 70.7 μm.
[c]A 50-mm aspheric condenser lens was used to focus the laser pulses.
[d]Seven to nine pulses in a 25-ns pulse train were used.
[e]10 pulses in a 5-ns pulse train were used.

pers, especially the beam diameter at the focus and the cone angle, making comparison difficult. Many authors quote diffraction-limited spot sizes, which may not be physically reasonable because of aberrations, especially for short focal lengths and large cone angles. However, we will proceed to make some general comments regarding the differences in experimental conditions and then attempt to explain any important differences seen in shielding as the pulse duration is decreased.

The most obvious experimental difference between this study and past studies is the measured spot size at the focus. The spot size (diameter) for all of the past studies with the exception of Nahen[36] was equal to or greater than 25 μm. Another difference is the definition of threshold used by each author. Docchio and co-workers[24,31] used 100% probability of breakdown for the threshold. All other authors who precisely measured the threshold used 50% probability of breakdown. In addition, all past studies with the exception of Nahen's used an external lens to focus the beam into a cell or cuvette. This setup, which contains several interfaces with index mismatches, has been shown to introduce serious spherical aberrations,[39] although the aberrations are greater for more sharply focused beams than for beams with small cone angles and large spot diameters. There are similar interfaces in the eye, but they do not have very large index mismatches. With a large spot size and aberrations in the setup, multiple breakdown

sites are probable. Multiple breakdown sites lead to a decrease in the shielding because of the increased transmission between individual energy-absorption (breakdown) sites. Clinically, a large spot size is not an accurate model of the focusing characteristics used in intraocular surgery. The focused spot size (diameter) at or behind the posterior capsule during laser capsulotomy surgery for standard contact lenses was found to be less than 10 μm (Ref. 40).

Another difference is that most of the past studies concentrated on energies near or slightly above threshold. Although these energies may be those most often used by ophthalmologists in surgery, it is harder to distinguish clear trends in transmission between different pulse durations close to threshold. For example, for the present study at threshold ($\beta = 1$), there is little difference between the transmission percentages, and the true trends do not become apparent until higher energies are reached.

There are also differences in the experimental conditions that probably do not play an important role in the shielding trends. For all past studies with the exception of Boppart *et al.*[29] and Steinert *et al.*,[28] the wavelength of the laser was 1064 nm (Docchio and Sacchi reported the breakdown thresholds at 532 nm but did not report the shielding at this wavelength[24]). We used visible (532 and 580 nm) pulses to allow comparison of nanosecond to femtosecond pulse durations, and measurements by Nahen[36] at 1064 nm support the trend reported in this paper at visible wavelengths. Steinert also found little difference in shielding at 15 ns between 1064-nm and 532-nm laser pulses. In addition, the media used in the various studies were slightly different. The choice of media has been shown to cause a difference in the breakdown threshold for nanosecond pulses since avalanche ionization is impurity dependent.[41,42] Variations caused by impurities in both the shielding percentage with respect to energy normalized by threshold (β) and the shielding trends with respect to pulse duration are probably not significant.

There are some general trends in each paper that will now be highlighted, beginning with a restatement of the trends found in this paper. As can be seen from Table 2, which lists the transmission for $\beta = 1$ and $\beta = 2$, the shielding decreases (transmission increases) from 5 ns to 300 fs and increases (transmission decreases) from 300 fs to 125 fs. The decrease in shielding from nanosecond to picosecond was also seen by three authors, Mainster *et al.*,[29] Nahen,[36] and Steinert *et al.*,[28] although Mainster and Steinert both used a train of picosecond pulses, instead of single picosecond pulses used in this paper. Mainster had extraordinarily low transmission values at threshold, which may be attributed to the cone angle at which he collected the transmitted light or perhaps to other experimental factors unknown to us.

Boppart *et al.*,[29] Chekelin and Mishakov,[25] and Docchio *et al.*[31] all report trends that differ from those found in this paper. In fact, Boppart also reported the exact opposite trend from picosecond to femtosecond pulse durations, namely, a decrease in shielding (increase in transmission), whereas we have found an increase in shielding from 300 fs to 125 fs.

The difference in shielding trends as reported by Boppart *et al.*[29] and those found in this paper are due to a number of different factors. Boppart did see an increase in transmission of the 100-fs data in comparison with the 10-ns data. Also, the percent transmission values he found for 100-fs and 10-ns pulses at $\beta = 1$ are within the error bars of those found for 125-fs and 5-ns pulses at $\beta = 2$ in this paper. Thus the difference for nanosecond and femtosecond shielding was probably due to either an error in threshold measurement or an inaccurate accounting of energy. For picosecond pulses there is a much larger difference in shielding. It is not known why this difference occurred.

Chekelin and Mishakov[25] found very high shielding for picosecond pulses. However, they also reported a different threshold for shock wave generation and optical breakdown in water. Since absorption and shock wave generation occur because of optical breakdown, a shock wave threshold below a breakdown threshold does not agree with current evidence of LIB and cavitation dynamics. In addition, they listed a breakdown threshold of 3.6 ± 0.15 mJ but also presented data at 50 mJ for which no breakdown occurred. We believe there may have been a difference in the method by which they measured the threshold compared with our method. Therefore a critical comparison between our data and those of Chekelin and Mishakov is not possible.

The final comparison to be made is with the author most commonly cited regarding shielding. Docchio and co-workers have done a great deal of laudable work on laser-induced breakdown. However, there are many pieces of information missing from their papers and discrepancies that make comparison difficult. For example, in their first paper on shielding,[31] Docchio *et al.* list the transmission at 7 ns at threshold as 45%. But in the study comparing different pulse durations,[24] Docchio and Sacchi list the transmission at 7 ns at threshold as 57%. In addition, the abstract to their second paper on shielding[24] lists thresholds and transmission values that are inconsistent with those listed in the body of the paper. Also, this paper does not mention a spot size or a focal length for the lens used to focus the laser beam into the cuvette. Moreover, Docchio and Sacchi looked at only a few data points above twice the breakdown threshold. Had their data been extended to large values of β, further information might have been obtained from these papers. Assuming these to be minor errors, the difference in the trends of Docchio and co-workers should be explained with the same reasoning used above for those of Boppart *et al.*, namely, a discrepancy in energy threshold measurement and an inaccurate accounting of energy throughput led to an apparent increase in shielding percentage for picosecond pulses with respect to nanosecond pulses.

B. Decreased Shielding Efficiency from Nanosecond to Picosecond: Electron Density

In the papers reviewed in the preceding subsection there is some discussion but little explanation of the trends reported for shielding. In this and the following subsection we present physical hypotheses on the shielding efficiency trends found from the experimental measurements reported in this paper. This subsection puts forth an explanation for the decreased shielding efficiency as pulse duration decreases from 5 ns to 300 fs. In the next subsection we explain the increased shielding efficiency as pulse duration decreases from 300 to 125 fs.

The decreased shielding efficiency as pulse duration is decreased from 5 ns to 300 fs can be linked to a decrease in plasma electron density. Plasma spectroscopy has shown evidence that the electron density after breakdown decreases as the pulse duration decreases. For example, it has been found that the plasma temperature decreases as the pulse duration decreases from nanosecond pulses to picosecond pulses.[15] Furthermore, for pulses less than 10 ps, there is an absence of visible plasma light altogether.[39,43] Since the fractional ionization (ions/molecules) decreases as the plasma temperature decreases,[42] the free-electron density will decrease as well.

The mechanism for plasma shielding is inverse bremsstrahlung absorption of photons during collisions between electrons and heavy particles (molecules or ions). Lower electron densities will thus lead to a lower absorption rate per volume and less efficient shielding unless compensated by some other factor. One factor that could compensate for the decreased electron density is a larger plasma volume (which is determined mostly by the plasma length, especially for the long, thin, femtosecond plasmas). Vogel found that for equal β, the plasma length of nanosecond pulses is considerably longer than the plasma length of picosecond pulses for equal β (Fig. 4 of Ref. 11). Therefore the measured decrease in shielding can be attributed to lower electron densities within the plasma.

In gas plasmas, inverse bremsstrahlung absorption becomes less efficient with a large decrease in the electron–ion collision frequency, and resonance absorption begins to affect light absorption in the plasma.[44] Resonance absorption is a condition in which obliquely incident electromagnetic waves are linearly converted into plasma waves in the presence of local plasma-density inhomogeneities. Experimentation and numerical simulation have found that the peak resonance absorption is approximately 0.5, with reflection and transmission each 0.25 (Refs. 44 and 45). The value for transmission corresponds approximately to the values for large β and pulse durations shorter than 3 ps found in this paper. Further theoretical work for plasmas in liquids is necessary to verify the effect of resonance absorption in the current configuration.

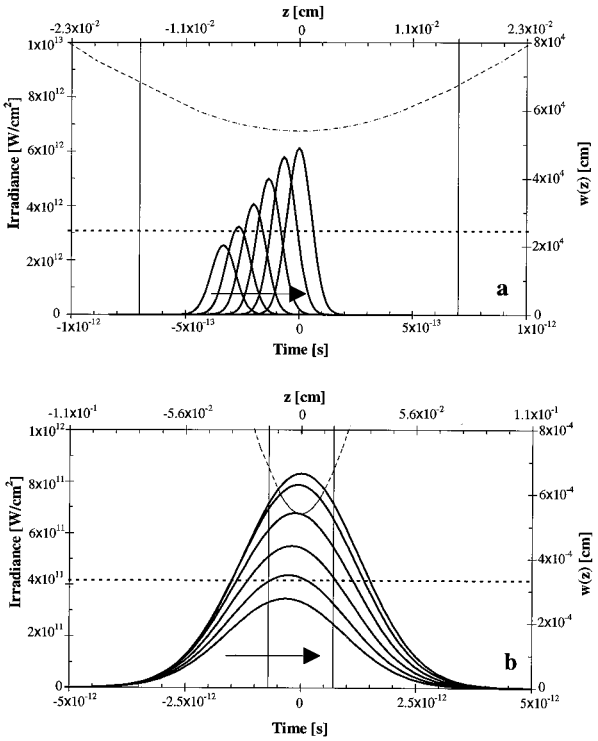

Fig. 5. Sequence of irradiance profiles (thick solid curves) of the pulse is plotted as a function of time on the lower and left axes and the spatial profile (thin dashed curve) is plotted on the upper and right axes for, a, 125 fs and, b, 3 ps. The irradiance profiles are from Eq. (2) and the spatial profile is from Eq. (3). Time on the lower axes corresponds to the distance over which light travels on the upper axes. The vertical lines denote the Rayleigh range, and the horizontal line denotes the breakdown threshold. The arrows indicate the direction of pulse propagation.

C. Increased Shielding Efficiency from Picosecond to Femtosecond: Moving-Breakdown Model and Nonlinear Effects

We offer two explanations for the increase in shielding efficiency from 3-ps and 300-fs pulses to 125-fs pulses, the moving-breakdown model[46,47] and nonlinear effects. The moving-breakdown model is merely a description of the pulse in time as it travels through space. It assumes only one condition for breakdown, that the irradiance measured as a function of time and space is greater than the breakdown-irradiance threshold. The model indicates a reversal in the direction the breakdown progresses with respect to pulse duration as the pulse travels through the focal region. Nonlinear effects that occur only at very short pulse durations (<1 ps) can have an effect on the amount of light that is absorbed in the plasma, and hence the efficiency of shielding. Self-focusing and continuum generation will be briefly discussed as possible explanations for the increased shielding seen at 125 fs.

Figure 5 illustrates the concepts of the moving-breakdown model. A sequence of irradiance profiles, $I(z, t)$, is plotted as a function of time, t, and distance from focus, z, of a Gaussian pulse of duration

125 fs [Fig. 5(a)] and 3 ps [Fig. 5(b)], according to

$$I(z, t) = \frac{E}{\pi\omega^2(z)\tau}\{\exp[-2(tA/2\tau)^2]\}, \quad (2)$$

where E is energy (in joules), $\omega(z)$ is the radius of the spot (in centimeters), τ is the pulse duration (in seconds), and A is defined to be $2(2 \ln 2)^2$. Each temporal profile is separated by 50 μm (corresponding to 222 fs in water). The energy chosen for the curves in Fig. 5 was twice the measured threshold ($\beta = 2$), and the diffraction-limited spot (radius) at the beam focus was assumed to be 5.4 μm. The left and lower axes correspond to the irradiance profile as a function of time. The thin dashed curve in Fig. 5 is the spatial profile (beam radius) as a function of distance from the focus according to

$$\omega(z) = \left(\omega_0^2\left\{1 + \left[\frac{\lambda_0(z - z_0)}{\pi\omega_0^2 n_0}\right]^2\right\}\right)^{1/2}, \quad (3)$$

where λ_0 is the wavelength (in centimeters), n_0 is the index of refraction (unitless), ω_0 is the radius at the waist (in centimeters), and z_0 is the location of the beam waist (in centimeters). Diffraction-limited focusing is assumed for this discussion. The right and upper axes correspond to the spatial profile. The distance on the upper axis corresponds to the time over which light travels on the lower axis. The vertical lines indicate the Rayleigh range, and the horizontal line indicates the irradiance threshold for breakdown. Note the difference in temporal dimensions between 125 fs and 3 ps. Also note that when the 3-ps pulse reaches breakdown it does so at approximately the same time within the entire Rayleigh range but the 125-fs pulse can reach breakdown in the Rayleigh range well before the pulse has reached the minimum focus.

The moving breakdown model assumes that breakdown occurs independently at every point along the axis as long as the irradiance (in watts per square centimeter) at that point exceeds the threshold irradiance. For 3-ps pulses [Fig. 5(b)] and longer, the irradiance at the minimum beam diameter will reach threshold essentially before any other point along the axis because of the temporal extent of the profile. Thus breakdown is predicted to begin at the beam waist and to move back toward the laser during the pulse (in the opposite direction of pulse propagation). For femtosecond pulses, however, this is not the case [Fig. 5(a)]. The irradiance may exceed breakdown threshold prior to reaching the beam waist owing to the narrow temporal profile of femtosecond pulses (light travels only 28 μm in 125 fs in water, a distance smaller than the Rayleigh range). For femtosecond pulses, breakdown is predicted to begin before the beam waist and to move forward to the focal plane during the pulse (in the direction of pulse propagation).

At approximately 1.4 ps (for a spot diameter of 10.8 μm), our calculation using the moving-breakdown model predicts a reversal in the direction the breakdown progresses as the pulse propagates through the focal volume. Thus, for long pulse durations (5 ns), the spatial dependence of the irradiance dominates, and the maximum irradiance is always at the beam waist. However, for short pulse durations (125 fs), the temporal dependence of the irradiance dominates, and the irradiance may not be largest at the beam waist at a given time. Breakdown and shielding may occur before the pulse reaches a minimum diameter.

In the region where the temporal profile dominates (<1.4 ps), shielding efficiency was found to be greater for shorter pulse durations than longer pulse durations. It may be possible that, owing to the larger temporal extent of the pulse, a larger portion of the pulse energy is transmitted for 3-ps pulses than for 125-fs pulses. Thus greater efficiency may be achieved for the 125-fs pulse because the shielding occurs as the pulse propagates forward and the breakdown region propagates with the pulse, producing increased absorption. However, the curves in Fig. 5 are drawn without consideration of how they will be altered by the plasma formation itself. A measurement of the temporal profile of the pulse as it passes through the focal region and is absorbed by the plasma would give further insight into this hypothesis. At the present time, such a measurement is technically not feasible.

Other factors that may explain the increased shielding for 125 fs are nonlinear effects, including self-focusing and continuum generation. Self-focusing occurs in aqueous solutions because of the effect of its nonlinear index of refraction. This effect is proportional to the square of the electric-field intensity. Thus self-focusing is readily seen for very short pulse durations. The critical power for self-focusing (P_{cr}) is related to the linear and the nonlinear refractive indices (n_0 and n_2) and the wavelength (λ_0) according to[48]

$$P_{\mathrm{cr}} = \frac{0.159\lambda_0^2}{n_0 n_2}. \quad (4)$$

The critical power for self-focusing in water at 580 nm calculated from Eq. (4) is 1 MW (Ref. 48). Considering the values of the laser power at which breakdown occurs (0.37 MW, 3.3 MW, and 3.5 MW for 3 ps, 300 fs, and 125 fs, respectively), it is clear that between 3 ps and 300 fs the threshold where self-focusing significantly affects pulse propagation is crossed.

Continuum generation or self-phase modulation also occurs because of the effect of the nonlinear index of refraction of materials. Because of the change in refractive index of the material a time-dependent phase advance or retardation occurs, which in turn causes spectral broadening. For femtosecond pulses, the spectral broadening can encompass the entire visible range. For 125-fs pulses, up to approximately 10% of the input energy is converted into broadband light for large values of β. It is not known at this time exactly how self-focusing and continuum generation affect the shielding.

These observations of shielding efficiency suggest that laser-induced breakdown induced by ultrashort pulses (<1 ps) is different from breakdown from pulses of longer duration. Other differences have been shown to exist. For example, the first-order breakdown model developed by Kennedy and coworkers[41,42] predicts a change in dominant breakdown mechanism from avalanche ionization to multiphoton ionization below 1 ps. Also, as mentioned above, it has been reported that there is an absence of the typical luminescence or spark for pulse durations of 3 ps and below.[39,43] Time-resolved and streak imaging have shown the shape of the plasma at nanosecond pulse durations to be quite different than those for femtosecond pulse durations. In addition, nonlinear dispersion becomes significant in this regime. Not all of these factors may contribute directly to increased shielding in the femtosecond regime; however, they all may play key roles in the sequence of physical phenomena associated with LIB for pulses less than 1 ps.

D. Implications for Ophthalmic Surgery

The shielding trends measured in this paper have important implications if ultrashort (femtosecond and picosecond) pulses are to be used in ophthalmic surgery to reduce the collateral damage now associated with nanosecond pulses. It is especially critical that the light that reaches the retina remains below the threshold for damage. The radiant exposure damage threshold for 90-fs, 580-nm pulses in rhesus monkeys was measured to be approximately 1 $\mu J/cm^2$ (Ref. 49). Therefore femtosecond pulses focused at breakdown threshold energies at structures in the anterior portion of the eye are less dangerous in terms of radiant exposure than nanosecond pulses with similar focusing characteristics. However, nonlinear effects can seriously alter the pulse profile and focusing characteristics as the pulses become shorter; 125-fs pulses provide greater shielding than 3-ps pulses, but the critical power for self-focusing occurs at a lower energy. When the threshold for self-focusing is surpassed, beam reduction and filamentation can occur. This in turn can lead to higher energy densities beyond the focus. In addition, continuum generation can create an additional hazard at the retina that is due to different wavelengths, possibly even ultraviolet wavelengths, which are normally blocked from the retina by the cornea and the lens. The shielding effectiveness at a particular pulse duration is then just one factor among many to be considered when choosing the best pulse duration for safety, optimization of cutting, and a reduction of collateral damage.

5. Conclusion

We have observed that the shielding efficiency decreases from 5 ns to 300 fs. A hypothesis for this trend has been described: A lower electron density for picosecond pulses leads to a lower probability of absorption of a photon by an electron and hence less efficient shielding. Moreover, we have observed that the shielding efficiency increases from 300 fs to 125 fs. Two hypotheses have been offered to explain this trend: the moving-breakdown model and nonlinear effects. The moving-breakdown model predicts a reversal in the direction in which the plasma moves, and this reversal may lead to increased shielding because the entire pulse is exposed to the breakdown for 125-fs pulses, whereas for longer pulses a significant amount of energy may pass the focal volume before it is shielded. Self-focusing and continuum generation change the spatial and temporal profiles of the pulse as it propagates through the focal volume. These nonlinear effects probably have an influence on the amount of energy absorbed in the plasma.

The authors acknowledge the support of the U.S. Air Force Office of Scientific Research (contract 2312AA-92AL014), the U.S. Air Force (contract F33615-92-C-0017), the Albert and Clemmie Caster Foundation, the Office of Naval Research (contract N00014-91-J1564), the German Research Foundation (grant Bi312/2-4), the German Science Foundation (grant Fr1147/1-1), the National Research Council, and Armstrong Laboratory. The authors thank Paul Kennedy and Clarence Cain for helpful discussions.

References

1. D. Aron-Rosa, J. J. Aron, M. Griesemann, and R. Thyzel, "Use of the neodymium-YAG laser to open the posterior capsule after lens implant surgery: a preliminary report," J. Am. Intraoc. Implant Soc. **6,** 352–354 (1980).
2. F. Fankhauser, J. S. Roussel, E. van der Zypen, and A. Chrenkova, "Clinical studies on the efficiency of high power laser radiation upon some structures of the anterior segment of the eye," Int. Ophthalmol. Clin. **3,** 129–139 (1981).
3. F. Fankhauser, H. Lortscher, and E. van der Zypen, "Clinical studies on high and low power laser radiation upon some structures of the anterior and posterior segments of the eye," Int. Ophthalmol. Clin. **5,** 15–32 (1982).
4. A. C. Terry, W. J. Stark, A. E. Maumenee, and W. Fagadau, "Neodymium-YAG laser for posterior capsulotomy," Am. J. Ophthalmol. **96,** 716–720 (1983).
5. R. M. Klapper, "*Q*-switched neodymium: YAG laser iridotomy," Ophthalmology **91,** 1017–1021 (1984).
6. M. M. Krasnov, "Laseropuncture of anterior chamber angle in glaucoma," Am. J. Ophthalmol. **75,** 674–678 (1973).
7. E. van der Zypen, F. Fankhauser, H. Bebie, and J. Marshall, "Changes in the ultrastructure of the iris after irradiation with intense light," Adv. Ophthalmol. **39,** 59–180 (1979).
8. D. X. Hammer, G. D. Noojin, R. J. Thomas, C. E. Clary, B. A. Rockwell, C. A. Toth, and W. P. Roach, "Intraocular laser surgical probe (ILSP) for membrane ablation by laser-induced breakdown," Appl. Opt. **36,** 1684–1693 (1997).
9. P. Teng, N. S. Nishioka, R. R. Anderson, and T. F. Deutsch, "Optical studies of pulsed laser fragmentation of biliary calculi," Appl. Phys. B **42,** 73–78 (1987).
10. S. J. Gitomer and R. D. Jones, "Laser-produced plasmas in medicine," IEEE Trans. Plasma Sci. **19,** 1209–1219 (1991).
11. A. Vogel, "Non-linear absorption: intraocular microsurgery and laser lithotripsy," Phys. Med. Biol. **42,** 1–18 (1997).
12. M. J. C. van Gemert and A. J. Welch, "Clinical use of laser-tissue interactions," Eng. Med. Biol. **8,** 10–13 (1989).
13. Y. Ito, O. Ueki, and S. Nakamura, "Determination of colloidal iron in water by laser-induced breakdown spectroscopy," Anal. Chim. Acta **299,** 401–405 (1995).
14. K. Mansour, M. J. Soileau, and E. W. Van Stryland, "Nonlinear

optical properties of carbon-black suspensions (ink)," J. Opt. Soc. Am. B **9,** 1100–1109 (1992).
15. R. J. Thomas, D. X. Hammer, B. A. Rockwell, G. D. Noojin, D. J. Stolarski, and W. P. Roach, "Spectroscopy measurements of laser-induced breakdown in water," submitted to J. Opt. Soc. Am. B.
16. A. Vogel, S. Busch, K. Jungnickel, and R. Birngruber, "Mechanisms of intraocular photodisruption with picosecond and nanosecond laser pulses," Lasers Surg. Med. **15,** 32–43 (1994).
17. A. Vogel and W. Lauterborn, "Acoustic transient generation by laser-produced cavitation bubbles near solid boundaries," J. Acoust. Soc. Am. **84,** 719–731 (1987).
18. A. Vogel, P. Schweiger, A. Frieser, M. Asiyo, and R. Birngruber, "Intraocular Nd:YAG laser surgery: damage mechanisms, damage range and reduction of collateral effects," IEEE J. Quantum Electron. **QE-26,** 2240–2259 (1990).
19. A. Vogel, M. Capon, M. Asiyo-Vogel, and R. Birngruber, "Intraocular photodisruption with picosecond and nanosecond laser pulses: tissue effects in cornea, lens, and retina," Invest. Ophthalmol. Vis. Sci. **35,** 3032–3044 (1994).
20. F. Docchio, L. Dossi, and C. A. Sacchi, "*Q*-switched Nd:YAG laser irradiation of the eye and related phenomena: an experimental study. III. Experimental observation of stimulated Brillouin scattering in eye models," Lasers Life Sci. **1,** 117–124 (1986).
21. G. G. Luther, J. V. Moloney, A. C. Newell, and E. M. Wright, "Self-focusing threshold in normally dispersive media," Opt. Lett. **19,** 862–864 (1994).
22. Q. Z. Wang, P. P. Ho, and R. R. Alfano, "Supercontinuum generation in condensed matter," in *The Supercontinuum Laser Source*, R. R. Alfano, ed. (Springer-Verlag, New York, 1989), pp. 33–90.
23. A. Vogel, S. Busch, and U. Parlitz, "Shock wave emission and cavitation bubble generation by picosecond and nanosecond optical breakdown in water," J. Acoust. Soc. Am. **100,** 148–165 (1996).
24. F. Docchio and C. A. Sacchi, "Shielding properties of laser-induced plasmas in ocular media irradiated by single Nd:YAG pulses of different durations," Invest. Ophthalmol. Vis. Sci. **29,** 437–443 (1988).
25. S. V. Chekalin and G. V. Mishakov, "Role of laser-induced shock waves and specifics of perforation of a cellular monolayer in water by an ultrashort pulse," Lasers Life Sci. **2,** 173–184 (1988).
26. R. H. Hora, H. G. L. Coster, C. J. Walter, and H. Hora, "Self-focusing limits at the laser-plasma interactions for the treatment of cataract with nanosecond and picosecond pulses," Laser Part. Beams **10,** 163–178 (1992).
27. B. Zysset, J. G. Fujimoto, C. A. Puliafito, R. Birngruber, and T. F. Deutsch, "Picosecond optical breakdown: tissue effects and reduction of collateral damage," Lasers Surg. Med. **9,** 193–204 (1989).
28. R. F. Steinert, C. A. Puliafito, and C. Kittrell, "Plasma shielding by *Q*-switched and mode-locked Nd-YAG lasers," Ophthalmology **90,** 1003–1006 (1983).
29. S. A. Boppart, C. A. Toth, W. P. Roach, and B. A. Rockwell, "Shielding effectiveness of femtosecond laser-induced plasmas in ultrapure water," in *Laser-Tissue Interaction IV*, S. L. Jacques, ed., Proc. SPIE **1882,** 347–354 (1993).
30. M. R. C. Capon, F. Docchio, and J. Mellerio, "Nd:YAG laser photodisruption: an experimental investigation on shielding and multiple plasma formation," Graefe's Arch. Clin. Exp. Ophthalmol. **226,** 362–366 (1988).
31. F. Docchio, L. Dossi, and C. A. Sacchi, "*Q*-switched Nd:YAG laser irradiation of the eye and related phenomena: an experimental study. II. Shielding properties of laser-induced plasmas in liquids and membranes," Lasers Life Sci. **1,** 105–116 (1986).
32. M. A. Mainster, D. H. Sliney, C. D. Belcher, and S. M. Buzney, "Laser photodisruptors. Damage mechanisms, instrument design and safety," Ophthalmology **90,** 973–991 (1983).
33. R. U. Orlov, I. B. Skidan, and L. S. Telegin, "Investigation of breakdown produced in dielectrics by ultrashort laser pulses," Sov. Phys. JETP **34,** 418–421 (1972).
34. C. A. Puliafito and R. F. Steinert, "Laser surgery of the lens. Experimental studies," Ophthalmology **90,** 1007–1012 (1983).
35. R. F. Steinert, C. A. Puliafito, and S. Trokel, "Plasma formation and shielding by three ophthalmic neodymium-YAG lasers," Am. J. Ophthalmol. **96,** 427–434 (1983).
36. K. Nahen, "Investigations on plasma formation in water by nanosecond and picosecond Nd:YAG laser pulses," Masters thesis (Medical Laser Center Lübeck and University of Hamburg, Lübeck, 1996).
37. A. E. Siegman, M. W. Sasnett, and T. F. Johnston, "Choice of clip levels for beam width measurements using knife-edge techniques," IEEE J. Quantum Electron. **QE-27,** 1098–1104 (1991).
38. D. X. Hammer, R. J. Thomas, M. Frenz, E. D. Jansen, G. D. Noojin, S. J. Diggs, J. Noack, A. Vogel, and B. A. Rockwell, "Shock wave and cavitation bubble measurements of ultrashort pulse laser-induced breakdown in water," in *Laser-Tissue Interactions VII*, S. L. Jacques, ed., Proc. SPIE **2681,** 437–448 (1996).
39. D. X. Hammer, R. J. Thomas, G. D. Noojin, B. A. Rockwell, and A. Vogel, "Ultrashort pulse laser-induced bubble creation thresholds in ocular media," in *Laser-Tissue Interactions VI*, S. L. Jacques, ed., Proc. SPIE **2391,** 30–40 (1995).
40. P. Rol, F. Fankhauser, and S. Kwasniewska, "Evaluation of contact lenses for laser therapy, part I," Lasers Ophthalmol. **1,** 1–20 (1986).
41. P. K. Kennedy, S. A. Boppart, D. X. Hammer, B. A. Rockwell, G. D. Noojin, and W. P. Roach, "A first-order model for the computation of laser-induced breakdown thresholds in ocular and aqueous media: Part II—Comparison to experiment," IEEE J. Quantum Electron. **QE-31,** 2250–2257 (1995).
42. P. K. Kennedy, "A first-order model for the computation of laser-induced breakdown thresholds in ocular and aqueous media: Part I—Theory," IEEE J. Quantum Electron. **QE-31,** 2241–2249 (1995).
43. D. X. Hammer, R. J. Thomas, G. D. Noojin, B. A. Rockwell, P. K. Kennedy, and W. P. Roach, "Experimental investigation of ultrashort pulse laser-induced breakdown thresholds in aqueous media," IEEE J. Quantum Electron. **QE-32,** 670–678 (1996).
44. K. G. Estabrook, E. J. Valeo, and W. L. Kruer, "Two-dimensional relativistic simulations of resonance absorption," Phys. Fluids **18,** 1151–1159 (1975).
45. W. L. Kruer, *The Physics of Laser Plasma Interactions* (Addison-Wesley, Redwood City, Calif., 1988), Chap. 4, pp. 37–43.
46. F. Docchio, P. Regondi, M. R. C. Capon, and J. Mellerio, "Study of the temporal and spatial dynamics of plasmas induced in liquids by nanosecond Nd:YAG laser pulses. 1: Analysis of the plasma starting times," Appl. Opt. **27,** 3661–3668 (1988).
47. F. Docchio, P. Regondi, M. R. C. Capon, and J. Mellerio, "Study of the temporal and spatial dynamics of plasmas induced in liquids by nanosecond Nd:YAG laser pulses. 2: Plasma luminescence and shielding," Appl. Opt. **27,** 3669–3674 (1988).
48. Q. Feng, J. V. Moloney, A. C. Newell, E. M. Wright, K. Cook, P. K. Kennedy, D. X. Hammer, B. A. Rockwell, and C. R. Thompson, "Theory and simulation on the threshold of water breakdown induced by focused ultrashort laser pulses," IEEE J. Quantum Electron. **QE-33,** 127–137 (1997).
49. C. P. Cain, C. A. Toth, C. D. DiCarlo, C. D. Stein, G. D. Noojin, D. J. Stolarski, and W. P. Roach, "Visible retinal lesions from ultrashort laser pulses in the primate eye," Invest. Ophthalmol. Vis. Sci. **36,** 879–888 (1995).